Novel centroid method for robust evaluation of return time of reflected waves in the systemic arterial network

Avinash Kondiboyina[1,2], Joseph J. Smolich[1,2], Michael M.H. Cheung[1,2,3], Jonathan P Mynard[1,2,4]

[1]Heart Research, Murdoch Children's Research Institute, Parkville, VIC, Australia

[2]Department of Paediatrics, University of Melbourne, Parkville, VIC, Australia

[3]Department of Cardiology, Royal Children's Hospital, Parkville, VIC, Australia

[4]Department of Biomedical Engineering, University of Melbourne, Parkville, VIC, Australia

Running title: Reflected wave return time with a centroid method

Corresponding author:

Jonathan Mynard, PhD

Heart Research

Murdoch Children's Research Institute

50 Flemington Rd. Parkville, VIC, Australia

Email: jonathan.mynard@mcri.edu.au

Abstract

Arterial ageing is thought to cause a diastolic-to-systolic shift in the return time (RT) of backward waves to central arteries. However, current methods of estimating RT—inflection point, zero crossing, and foot methods—depend on a single waveform feature and produce systolic RT throughout life. We propose a novel centroid method that accounts for the entire backward pressure waveform and develop a ground truth RT (GTRT), which can be used in computational models to test the accuracy of RT estimation methods. Linear wave tracking was implemented in a one-dimensional systemic arterial tree model and GTRT was calculated as the amplitude-weighted mean RT of backward waves at the ascending aorta. Using a virtual cohort of 1200 patients, the centroid RT was closest to GTRT compared to the zero crossing, inflection point, and foot methods; mean differences (limits of agreement) were -8 (-47,30), vs -42 (-136,52), -78 (-305,149), and -197 (-379,-15) ms, respectively. The sensitivity of the methods to changes in RT was also assessed in ten sheep. A balloon catheter in the descending thoracic aorta was used to generate a backward-running pulse that arrived at the ascending aorta at different times during diastole or systole, allowing the "bulk" RT of the backward-running wave ensemble to be manipulated. Only the centroid method was sensitive to both diastolic and systolic changes in RT. We conclude that the accuracy and robustness of the centroid method make it most suitable for evaluating the diastolic-to-systolic shift in RT of backward waves with ageing.

Keywords: wave reflection; cardiovascular modelling; arterial hemodynamics

New & Noteworthy

There is an expected diastolic-to-systolic shift in return time with ageing; however, current methods show systolic return times throughout life. We presented a novel centroid method that estimates return time by uniquely accounting for the distributed nature of wave reflection. Using a ground truth return time developed using computational methods, we showed that the centroid method provided the most accurate return times and, unlike other methods, was sensitive to both diastolic and systolic return times.

Introduction

As the left ventricle starts ejecting, it generates a forward-travelling pressure wave that is reflected at various sites of impedance mismatch in the vasculature. The resulting multitude of backward waves return to the ventricle throughout the cardiac cycle (1)—at different times (depending on the wave propagation speed and the distance from various reflection sites) and with different magnitudes (depending on the degree of reflection). The return time of these waves to the ventricle—whether during systole or diastole—is of importance because they predominantly exert a pressure-increasing effect (2). In youth, the backward waves are thought to return predominantly during diastole and cause diastolic augmentation of the ascending aortic pressure waveform, which supports coronary perfusion pressure (3-5). As arteries stiffen (e.g., with age), it is thought that backward waves return earlier, shifting the pressure augmentation from diastole to systole and increasing systolic pressure and left ventricular afterload (3-5). If left uncontrolled, increases in afterload can lead to left ventricular hypertrophy, which increases the risk of congestive heart failure (6). Thus, the change in return time of backward waves with vascular ageing not only helps explain the physiological changes observed in the central pressure waveform, but is also considered a critical aspect of pulsatile ventricular load with potential clinical value (7).

Although there are numerous backward waves of different magnitudes that return at different times because of the distributed nature of wave reflection, it is generally not possible to distinguish individual waves in vivo; therefore, a composite or ensemble "backward pressure waveform" composed of many individual backward waves is used to estimate the "bulk" return time. The most widely used method for estimating return time is

the inflection point method (8). The inflection point is a feature commonly visible in the systolic portion of central arterial blood pressure waveforms where the pressure temporarily plateaus and rises again. The inflection point is thought to indicate the time when the backward wave arrives and begins to augment pressure. A meta-analysis by Baksi et al. found that return times estimated by this method decreased with age but were well within systole throughout the lifespan, which is inconsistent with the traditional view that backward waves return predominantly in diastole in youth (9). In fact, the inflection point is calculated in such a way that it can never occur during diastole. Moreover, while wave reflection does give rise to the inflection point, it is also affected by factors independent of wave reflection such as ventricular outflow patterns (10). Thus, it may not provide an accurate representation of return time, which has indeed been the conclusion of several studies (11-14).

To improve the accuracy of estimated return time, other methods have been developed that involve extracting forward and backward pressure waveforms from the central pressure waveform using either frequency-domain (15) or time-domain methods (16). Two such methods include the zero crossing (17) and foot methods (18, 19), with both providing the same trend of decreasing return time with age as the inflection point method. However, both methods also produce return times well within systole (17, 18), making them also inconsistent with the paradigm of a diastolic-to-systolic shift in return time with ageing. Importantly, however, the accuracy of existing methods for estimating return time have not yet been rigorously evaluated, in part because there is no ‘ground truth’ for such an evaluation.

A key limitation of existing methods is that they rely on finding a single point on the waveform to estimate return time. This runs fundamentally counter to the composite nature of the

backward pressure waveform (i.e., there is no 'single' backward wave). Hence, taking the entire backward pressure waveform into account rather than a single point could better represent its composite nature, and provide clarity in the controversies about how return time changes with age. In this paper, we propose a novel "centroid method", in which the centroid of the entire backward pressure waveform is used to estimate an effective or 'bulk' return time of the backward wave ensemble.

The first aim of this study was therefore to rigorously investigate which method of estimating return time—centroid, zero crossing, inflection point, or foot method—provides the most accurate estimate of the bulk return time. Accuracy was evaluated by comparison with a ground truth return time (GTRT) obtained via a linear wave tracking algorithm applied in a one-dimensional model of the systemic arterial network. We hypothesized that the centroid method would provide a better estimate of return time than the other methods because it takes the composite nature of the backward pressure waveform into account. The second aim was to investigate the sensitivity of all methods to changes in return time, during both diastole and systole. Towards this, we conducted an experimental study in sheep where we introduced an artificially generated backward-travelling pressure pulse using an intra-aortic balloon pump. These pulses arrived at the ascending aorta at precisely controlled times in systole and diastole, hence changing the bulk return time. We hypothesized that only the centroid method, which accounts for the entire backward pressure waveform, would be sensitive to changes in wave reflection profile during both systole and diastole, because the other methods are based on single-point features found only in systole.

Methods

Wave Separation

The relationship between pressure and flow waves is described by the 'water hammer' equation (16, 20):

$$dP_{\pm} = \pm Z_c dQ_{\pm} \qquad \text{(Equation 1)}$$

where dP and dQ are wave-related changes in pressure and flow, respectively, Z_c is characteristic impedance, and the subscripts indicate direction of travel ('+' is forward and '−' is backward). Equation 1 indicates that forward waves cause pressure and flow to change in the same direction, while backward waves cause opposite changes. Thus, in the absence of wave reflection, the pressure waveform will be identical to the flow waveform (but scaled by characteristic impedance); therefore, wave reflection is entirely responsible for the difference between the waveforms observed in vivo.

Using Equation 1, the pressure waveform can be separated into forward (from the heart) and backward (towards the heart) pressure waveforms using the method proposed by Westerhof et al. (15), which requires the measurement of both pressure and flow waveforms:

$$P_{\pm} = \frac{P_m \pm Z_c Q_m}{2} \qquad \text{(Equation 2)}$$

where the subscript 'm' refers to the measured waveform and Z_c is calculated as the average value of the modulus of the 4th to 11th harmonic of the input impedance (17), which is the ratio of the Fourier transformed pressure and flow waveforms (15).

It is important to note that backward waves are re-reflected at the closed aortic valve during diastole and at the ventricle during systole when the aortic valve is open (21-24). Thus, the

forward pressure waveform (P_+) comprises both waves that are produced by active ventricular contraction (P_{+in}) and waves arising from re-reflection of backward waves. P_{+in} may therefore be considered the pressure that would exist in the absence of wave reflection, or the ventricular 'input' pressure to the arterial network; the best approximation of this is the flow waveform scaled by characteristic impedance ($Z_c \times Q$).

Methods of Estimating Return time

The zero crossing (17), inflection (25), and foot methods (19) have been described in detail elsewhere. Here we provide a brief description of each method and its implementation in the present study. The inflection point method only requires the pressure waveform, while the zero crossing and foot methods require both pressure and (measured or synthesized) flow waveforms because they involve wave separation analysis.

Inflection point: The dicrotic notch was first determined as the peak of the second derivative of the pressure waveform with the highest relative height (determined using 'findpeaks' function of MATLAB) after the maximum pressure (Figure 1a). The foot of the pressure waveform was found using the intersecting tangents method (26). The inflection point was then identified as the second derivative peak between the foot and dicrotic notch (17). The time difference between the foot and the inflection point was taken as the estimate of return time.

Zero crossing: As described by Segers et al, the pressure waveform was offset to zero mean and then separated into forward and backward pressure waveforms using wave separation in the frequency domain (17). The time difference between the zero crossings of the

backward and forward pressure waveforms was taken as the estimate of return time (Figure 1b).

Foot method: The pressure waveform was decomposed into forward and backward pressure waveforms using wave separation. The foot of the forward and backward pressure waveforms was found using the intersecting tangents method (19). However, in instances where the backward pressure waveform did not have a monotonic upstroke, the foot was instead taken as the minimum point of the backward pressure waveform. The time difference between the foot of the backward and forward pressure waveforms was taken as the estimate of return time (Figure 1c).

Centroid Method

The zero crossing and foot methods estimate return time using the backward pressure waveform (P_-) relative to a feature of P_+; however, as mentioned earlier, P_+ is influenced by re-reflections of the backward wave at the ventricle. To represent return time in terms of the actual pressure effect of backward waves, the centroid method therefore uses P_{+in}, the 'input' pressure to the arterial network without the influence of wave reflection ($Z_c \times Q$), instead of P_+. The centroid method estimates the bulk return time of backward waves using P_- and P_{+in}. Both waveforms are analyzed from the foot of one beat to that of the next. The foot of P_- is determined in the same manner as the foot method, and that of P_{+in} is determined using the intersecting tangents method. Minimum pressure is subtracted from P_- to better elucidate the influence of the shape of the waveform on its centroid. This is necessary because in the limit that the minimum pressure is very high, the time-axis centroid

will always be in the middle of the waveform, regardless of its shape. The time-axis centroids ($\bar{t}$) of P_{-} and P_{+in} are determined using the following formula:

$$\bar{t} = \frac{\int_a^b tP(t)dt}{\int_a^b P(t)dt} \qquad \text{(Equation 3)}$$

where a and b are the first and second foot of the waveform, respectively, $P(t)$ is the pressure waveform—either P_{-} or P_{+in}—and t is time. The difference between the time-axis centroids of P_{-} and P_{+in} is taken as the estimate of return time by the centroid method (Figure 2).

Linear Model

To assess the accuracy of these methods using a GTRT, every individual backward wave arriving at the ventricle must be tracked; this can only be achieved through computational methods. We recently developed and validated a non-linear one-dimensional model of the systemic arterial circulation of a young adult—the 'YoungAdult' model—the details of which are described elsewhere (27). In brief, a two-chamber heart model served as the input to the systemic arterial circulation, and distal arteries were terminated with 3-element windkessels representing vascular beds. Since all bifurcations in the arterial tree are thought to be relatively well-matched, with a reflection coefficient (R) of 0 in the forward direction (28), this was replicated in the YoungAdult model using a previously described optimization algorithm (27).

A linear wave tracking algorithm can enable tracking of every individual backward wave (29, 30), but it requires a linear model. Thus, the following modifications were made to the YoungAdult model to linearize it. The wave tracking algorithm requires a simple bifurcating

arterial tree; however, the cerebral arterial tree is looping in nature due to the circle of Willis. Hence, the cerebral arteries were replaced with a terminal windkessel to represent the cerebral vascular bed. Furthermore, the ventricle, arterial taper, and terminal windkessels were represented in a simplified form. First, the ventricle and aortic valve were assumed to be perfect reflectors of backward waves during systole and diastole, respectively. In reality, the value of R may change throughout the cardiac cycle; however, its precise value has not yet been determined but is thought to be close to 1 (24). Hence, the ventricle and aortic valve were removed and a constant value of $R = 1$ was imposed at the proximal end of the aorta. Second, tapered arteries (where employed) were discretized into 10 uniform segments of equal length, with successively decreasing area based on the degree of taper. Thus, there was a non-zero R at the junctions of successive segments, which represented the reflection properties of tapered vessels.

Finally, to account for the terminal windkessels, we initially replaced them with fractal arterial networks at every terminal vessel to represent the microvasculature. However, this increased the computation time exponentially. To improve efficiency, we used an R value at the distal end of the terminal vessels instead of the fractal network, which was calculated using the characteristic impedance of the terminal vessel (Z_{tv}) and the vascular bed resistance (R_{vb}):

$$R = \frac{R_{vb} - Z_{tv}}{R_{vb} + Z_{tv}} \qquad \text{(Equation 4)}$$

This did not significantly affect the results compared to the fractal network but dramatically improved the computation time (data not shown). This linearized form of the YoungAdult model is henceforth referred to as the LinearYoungAdult model. Wave attenuation due to viscous damping and the non-linearity introduced by the pressure-dependence of vessel wave

speed were not accounted for by the linear wave tracking algorithm. We have instead chosen to focus on the effect of complex arterial geometry on wave propagation in this study.

Linear Wave Tracking

To start the linear wave tracking algorithm using the LinearYoungAdult model, the heart model was removed and a forward-travelling impulse of amplitude 1 at time 0 was instead applied at the proximal end of the ascending aorta. The time taken for this impulse to 'traverse' the parent vessel was calculated by dividing the length of the vessel by its wave speed. At the distal end of the parent vessel where it bifurcated into two daughter vessels, the incident wave produced three waves: a backward wave traversing backwards through the parent vessel and a transmitted wave entering each of the daughter vessels. The ratio of backward to incident wave amplitudes was calculated via R:

$$R = \frac{\frac{A_0}{c_0} - \frac{A_1}{c_1} - \frac{A_2}{c_2}}{\frac{A_0}{c_0} + \frac{A_1}{c_1} + \frac{A_2}{c_2}} \qquad \text{(Equation 5)}$$

where A is vessel area, c is wave speed, the subscript 0 refers to parent vessel and subscripts 1 and 2 to the two daughter vessels. The ratio of transmitted to incident wave amplitudes (i.e., the transmission coefficient T) was equal in both daughter vessels and was calculated using the relationship $T = 1 + R$. A backward wave traversing through a parent vessel will be reflected into the parent vessel at its proximal end and transmitted into the 'grandparent' and 'sister' vessels (Figure 3). The R value at the proximal end of the parent vessel was again calculated using Equation 5, where subscript 0 now refers to the parent vessel and the subscripts 1 and 2 now refer to the grandparent and sister vessels. In this manner, the R values at the proximal and distal ends of every vessel were calculated, which helped

determine the amplitudes of the waves as they propagated through the network. In this manner, the timing and amplitude of every wave above an amplitude threshold (both forward and backward, see below) at the ascending aorta was kept track of, which was visualized by an impulse response (Figure 4a). Waves with positive and negative amplitudes exert a pressure-increasing (compression) and pressure-decreasing (decompression) effect, respectively. Finally, the amplitude-weighted mean time at which all backward waves (including both compression and decompression) returned to the inlet (within one cardiac cycle of 0.8 s) was taken as the GTRT.

Waveform Generation

To compare the various methods of estimating return time against GTRT, we need to apply them to waveforms from the linear wave tracking algorithm. Towards this, the ascending aortic flow waveform from the YoungAdult model was scaled by characteristic impedance (Z_c) to obtain P_{in+}, where Z_c was obtained by applying frequency-domain methods to the ascending aortic pressure and flow waveform of the YoungAdult model (3). P_{in+} was then convolved with the impulse response of the LinearYoungAdult model. The linear convolution of all forward and backward waves provided forward and backward pressure waveforms, respectively, which were then added to obtain the total pressure waveform (Figure 4b). Note that the pressure waveform is not as smooth as a measured waveform because the linear wave tracking algorithm does not account for attenuation of high frequency waves due to blood viscosity and wall viscoelasticity.

Amplitude Threshold

The amplitude threshold used for the linear wave tracking algorithm was determined by comparisons with the non-linear model. First, the cerebral arteries were excluded from the YoungAdult model to make it geometrically identical to the LinearYoungAdult model; the heart model and terminal windkessels were retained to maintain non-linearity. A previously described non-linear flow solver (31) was then applied to the YoungAdult model to obtain a pressure waveform at the ascending aorta. Comparison with the waveform obtained from the LinearYoungAdult model showed no further improvement in root mean square error below a threshold of 5.6×10^{-4}, and therefore this threshold was adopted throughout this study.

Virtual Cohort

To test the accuracy of the methods under a wide range of GTRT values, we created a virtual cohort using the LinearYoungAdult model by performing a parameter sweep of the following: R at every junction of the network, systemic vascular resistance, wave speed, and aortic taper. The same optimization algorithm used to match the junctions in the forward direction was used to change junction R values between -0.01 and 0.04 (32). Vascular resistance was varied between 0.5 and 1.5 mmHg.s.mL^{-1} by multiplying the resistance of all vascular beds by a factor to achieve the target systemic vascular resistance and modifying the distal R of terminal vessels accordingly (Equation 4). Wave speeds of all vessels in the model were multiplied by a factor between 0.5 and 3, resulting in aortic wave speeds covering a wide but physiological range of 2 to 14 m/s (33). Finally, while the baseline LinearYoungAdult model had no taper in any segment, the area of the ascending aorta is known to increase with age up to ~16 cm^2 (34). To assess the influence of aortic taper, we therefore simulated increases

in ascending aortic area from 6 to 16 cm^2, whilst keeping the area of the distal abdominal aorta constant and adjusting intervening aortic segments to achieve a linear taper (prior to discretization as described above). All combinations of junction R values (-0.01, 0, 0.01, 0.02, 0.03, and 0.04), vascular resistance (0.5, 0.75, 1, 1.25, and 1.5 $mmHg.s.mL^{-1}$), wave speed multiplier (0.5, 0.6, 0.7, 0.8, 0.9, 1, 1.5, 2, 2.5, and 3), and aortic taper (ascending aorta area: 5.94, 7.62, 10, and 16 cm^2) were used to create a virtual cohort of $6 \times 5 \times 10 \times 4 = 1200$ individuals.

Experimental Model

Methods for estimating return time were also evaluated in experimental studies performed in sheep. The protocol was approved by the Animal Ethics Committee of the Murdoch Children's Research Institute and conformed to the guidelines of the National Health and Medical Research Council of Australia. This manuscript is compliant with the ARRIVE guidelines for reporting of animal research.

Ten castrated male Border-Leicester cross sheep aged 12-15 months were anesthetized with an intramuscular injection of xylazine (0.05 mg/kg) and ketamine (5 mg/kg) followed by isoflurane (3-4%) in O_2 delivered by mask. After intubation of the trachea, anesthesia was maintained with a mixture of 1-3% isoflurane and nitrous oxide (10-20%) in oxygen-enriched air delivered via a ventilator (WATO EX-20Vet, Mindray, Shenzhen, China), and supplemented by an intravenous infusion of ketamine (1-1.5 mg/kg/hr), midazolam (0.1-0.15 mg/kg/hr), and fentanyl (2-2.5 μg/kg/hr) administered via a 7-Fr triple lumen catheter inserted into the right external jugular vein. Transcutaneous oxygen saturation (S_pO_2) was monitored continuously with a pulse-oximetry sensor applied to the ear. Through a neck incision, the right common

carotid artery was cannulated with a 5-Fr micromanometer catheter (SPC-454D; Millar Instruments, Houston, TX, USA) that was passed into the aortic root to obtain high-fidelity pressure and a 7-Fr vascular sheath for initial blood pressure monitoring and arterial sampling for blood gas analysis (ABL 800, Radiometer, Copenhagen, Denmark), with ventilation adjusted to maintain arterial O_2 tension (P_aO_2) at 100-120 mmHg and CO_2 tension (P_aCO_2) at 35-40 mmHg. Central temperature was monitored via a nasal thermistor probe and maintained at 38-39°C with a combination of heating pad and towel covering.

With animals in a right lateral position, a left thoracotomy was performed in the third intercostal space and the 2nd to 4th ribs removed to increase exposure of the heart and great arteries. A fluid-filled catheter was inserted into the proximal portion of the aortic arch via a purse-string suture to measure central aortic blood pressure via a transducer calibrated against a water manometer before each study and referenced to atmospheric pressure at the level of the thoracic spine. A 24 mm transit-time flow probe (Transonic Systems Inc, Ithaca, NY, USA) was placed around the ascending aorta to obtain cardiac output (minus coronary blood flow). A second 5-Fr micromanometer catheter was inserted into the left ventricle via the carotid artery sheath, and its signal was used to define beat onset using previously described methods (35). Catheter, micromanometer, and flow probe signals were digitized at a sampling rate of 1 kHz using programmable acquisition software (Spike2, Cambridge Electronic Design, Cambridge, UK).

Through an incision in the right groin, an intra-aortic balloon catheter (MEGA 8-Fr 50cc; Maquet Cardiovascular, Wayne, NJ, USA) was inserted via the right femoral artery and passed into the descending thoracic aorta. Using a custom-made triggering interface to precisely

control its timing, the balloon catheter was initially inflated at end diastole. This generated a backward-running pulse that travelled towards the ascending aorta, producing a prominent brief pulse in the ascending aortic pressure waveform. The timing of the pulse was then altered in a stepwise manner from end diastole to the start of systole (Figure 5). At each timestep, the balloon catheter was inflated once every 3 beats over approximately 30 beats.

Data Analysis

The time difference between the peak of the balloon-induced pulse ('BLIP') and the foot of the pressure waveform was called BLIP time. BLIP time was normalized to systolic duration (i.e. the time from the foot of the pressure waveform to the dicrotic notch), with the resulting quantity (BLIP Index) being less than 1 if occurring during systole and greater than 1 if occurring during diastole. Systolic duration was determined only once per animal when the BLIP arrived in late diastole because earlier arrival tended to obscure the dicrotic notch. Finally, as the BLIP time decreases, we expect a decrease in the apparent "bulk" return time of backward waves, given that the BLIP induces a backward wave. We used this to evaluate the sensitivity of the various methods for detecting changes in bulk backward wave return time during both systole and diastole.

To implement the centroid method using in vivo measurements, the flow waveform can be used as the input waveform and does not need to be scaled by characteristic impedance to obtain P_{in+}; this is because the time-axis centroid is unaffected by amplitude scaling. Furthermore, in vivo recordings of the flow waveform contain low level noise and fluctuations during diastole, when there is no aortic outflow. Flow and pressure waveforms were therefore first aligned, and the centroid of the flow waveform was then obtained by

considering only the region from its foot to the end of systole, marked by the dicrotic notch of the pressure waveform (Figure 2).

Statistical Analysis

To analyze the results of the virtual cohort, we used linear regression to determine the coefficient of correlation (r) between GTRT and estimated return time of the various methods; the corresponding degree of agreement was quantified by the intraclass correlation coefficient (ICC). We also used Bland-Altman analysis to evaluate the difference between GTRT and the various methods; the method that provided the least overall difference and limits of agreement was judged as the one with the highest accuracy and precision respectively. When plotting return time against BLIP Index for the sheep experiments, the zero crossing, inflection point, and foot methods had two visually distinct datasets, with the breakpoint (the boundary between the two datasets) approximately at a BLIP Index of 1. Thus, we performed segmented regression for all methods to precisely determine a breakpoint and analyse the two datasets separately. For each animal experiment, we iteratively selected the datapoints between 20% and 80% of the BLIP Index values as the breakpoints and performed linear regression on the two datasets produced. The datapoint that provided the lowest total error of the two resulting regressions was taken as the break point. We did not restrict the breakpoint analysis to a narrow band around a BLIP Index of 1 to limit visual bias and due to the lack of a visually discernible breakpoint for the centroid method. The break point analysis was performed for all 10 animals individually; the break point, regression intercept and slope, correlation coefficient, and p-value of all animals for a particular method were averaged to obtain the overall values. A method with a significant coefficient of correlation for both systolic and diastolic slopes was robust, in the sense that the method is sensitive to pulses

arriving in both systole and diastole. Data are reported as mean ± SD and a value of $p < 0.05$ was considered significant.

Results

Virtual Cohort

Data from the virtual cohort showed that the centroid method was closest to the identity line ($y = x$; Figure 6) and had the highest correlation and degree of agreement with GTRT [$r = 0.98$ and ICC = 0.98 (both $p < 0.001$)]. The zero crossing method also had good agreement with GTRT but (mostly) underestimated return time [$r = 0.93$ and ICC = 0.88 (both $p < 0.001$)]; it also had increased variability at larger GTRT values. Moreover, it performed better than the inflection point [$r = 0.38$ ($p < 0.001$) and ICC = 0.23 ($p = 0.0044$)] and foot methods [$r = 0.75$ ($p < 0.001$) and ICC = 0.17 ($p = 0.17$)]. Furthermore, the Bland-Altmann plots, with GTRT as the reference, showed that the centroid method had the lowest bias (highest accuracy) and tightest limits of agreement (highest precision) compared to the zero crossing, inflection point, and foot methods; mean differences (limits of agreement) were -8 ms (-47, 30), -42 ms (-136, 52), -78 ms (-305, 149), and -197 ms (-379, -15), respectively (Figure 7).

Animal Experiments

Table 1 presents the characteristics of the sheep included in the study. The break points for the centroid, zero crossing, inflection point, and foot methods were at a BLIP Index of 0.83, 1.35, 1.09, and 0.78, respectively (Figure 8). The zero crossing and inflection methods showed significant correlation with BLIP Index < 1 [i.e., systolic arrival, $r = 0.95$ ($p < 0.001$) and $r = 0.9$ ($p = 0.0031$), respectively] but no significant correlation for BLIP Index > 1 [i.e., diastolic arrival, $r = -0.43$ ($p = 0.28$) and $r = -0.11$ ($p = 0.49$), respectively]. The correlation for the foot method

did not reach significance during systole or diastole [r = 0.83 (p = 0.064) and r = 0.13 (p = 0.34), respectively]. Only the centroid method showed strong correlation with BLIP index during both systole (r = 0.96, p = 0.016) and diastole (r = 0.84, p = 0.014).

Discussion

We have proposed a novel centroid method for estimating the return time of backward waves that uniquely takes the composite nature of the backward pressure waveform into account. We have also for the first time rigorously described a GTRT to test the accuracy of various methods of estimating return time. Using the GTRT, results from the virtual cohort showed that the centroid method provided the most accurate and precise estimates of return time across a wide range of conditions compared to all other methods. Furthermore, sheep experiments showed that only the centroid method was sensitive to changes in both diastolic and systolic return times, with the other methods being sensitive only to systolic return times. We now discuss the drawbacks of other methods that explain their lower performance in this study and how the centroid method addresses them to provide more accurate and robust results.

The inflection point method is based on locating a fiducial point on the central pressure waveform that marks the point when backward waves begin to exert an influence on the pressure waveform. There are several limitations of this method that should be considered. First, the inflection point is found using the second derivative of the pressure waveform (17), making it highly susceptible to noise; furthermore, central pressure waveforms may not always have a distinct inflection point (36). Second, in reality many backward waves arise

from distributed reflection and return throughout the cardiac cycle; hence, finding a single point marking their return runs counter to their physiological behavior. Third, it has been shown that the inflection point is not a true marker of the return of backward waves because it is also influenced by factors such as ventricular outflow patterns (10), ejection duration (37), and heart rate (38). Finally, the inflection point is always found in systole throughout life (9), which is inconsistent with the expected diastolic-to-systolic shift in return time with ageing (3-5).

These limitations explain why the inflection point method did not estimate return times beyond 0.3 s (which was the systolic duration) in the virtual cohort and exhibited a low correlation with GTRT. They also explain the results of the sheep experiments, where the breakpoint was found at a BLIP Index of 1.03 (which corresponded to the boundary between systole and diastole). With a systolic arrival of BLIP (BLIP Index < 1), the BLIP created a prominent inflection point, which the inflection point method "locked onto". It thus gave a good correlation in this region and explains the high slope of the linear regression. With a diastolic arrival of BLIP (BLIP Index > 1), it just detected the natural inflection point of the pressure waveform during systole, which did not change with the timing of BLIP; thus, the inflection point method provided no correlation during diastole. The limitations of the inflection point method have led researchers to conclude that wave reflection metrics cannot be reliably obtained from the pressure waveform alone (10, 39); they suggest that wave separation using both pressure and flow waveforms should be used instead (3, 15, 40).

Wave separation decomposes the pressure waveform into forward (travelling away from the heart) and backward (travelling towards the heart) pressure waveforms. The backward

pressure waveform is produced entirely by wave reflection and is thus ideal for obtaining insights into the return time of backward waves. The foot method uses wave separation and estimates return time using the foot of the forward and backward pressure waveforms. This method shares some limitations with the inflection point method: 1) choosing a single point on the backward pressure waveform ignores its composite nature, and 2) the foot of the backward pressure waveform may not always be distinct, especially in case of noisy waveforms. The results of the virtual cohort suggest that an increase in GTRT did cause a slight increase in the timing of the foot of the backward pressure waveform, but not in a 1:1 manner (Figure 6), indicating the low accuracy of the foot method in estimating return time. The animal experiments showed that the foot method displayed marginal sensitivity to systolic arrival of BLIP, but it was insensitive to diastolic arrival. These findings are consistent with work by Torjesen et al., who showed that return times estimated by the foot method occur in systole over the entire adult age range (18).

The zero crossing method was introduced by Segers et al. and also uses wave separation (17). The results of the virtual cohort showed that this method provided good correlation with GTRT, although with some underestimation, but with variable error at large GTRT values. The animal experiments showed that, similar to the inflection point and foot methods, the zero crossing method was sensitive to changes in systolic arrival of BLIP, but not diastolic arrival. This was because it detected only the first zero crossing of the backward pressure waveform and was therefore unaffected by backward waves that returned later. This method has only been applied in participants 35-55 years of age, and only systolic return times were found (17).

In contrast to existing methods, the centroid method proposed in this paper accounts for the distributed nature of reflected waves and uses the entire backward pressure waveform rather than a single fiduciary point. Furthermore, since the centroid method accounts for the foot-to-foot area under the backward pressure waveform to determine its centroid, the exact location of the foot has little influence on the centroid, making it more robust than the foot method. This explains why it had a very high correlation with GTRT in the virtual cohort and was the only method that displayed good correlation with the BLIP timing across both systole and diastole in the animal experiments. The centroid method had a lower regression slope during systole compared to the inflection point and zero crossing methods. This is desirable in that the other methods "locked onto" the BLIP and were influenced entirely by the BLIP timing during systole, whereas the centroid return time was influenced by BLIP as well as other backward waves. These results indicate the greater robustness of the centroid method compared to other methods in representing bulk return time of reflected waves.

A major advance in this study was the description of a GTRT, which was obtained using linear wave tracking. This method has been previously used to explore the dynamics of wave propagation and reflection in the systemic arterial network (29, 30). The advantage of this approach is that it allows individual waves to be discretely tracked, which is necessary for obtaining a GTRT. One limitation of GTRT is that it did not account for the dispersion of waves that occur in vivo. This non-linear effect has a smoothing effect on the waveforms, but accounting for this phenomenon would make it difficult to track discrete waves and therefore calculate a GTRT.

A similar centroid method could also be used to quantify reflection magnitude. A study by Alastruey et al. defined a wave intensity reflection index as the ratio of the centroids of the backward and forward compression waves (41). However, Mynard et al. found that non-linear effects cause amplification or attenuation of wave intensity, leading to errors in indices of wave reflection, and potentially to values beyond the theoretical limits of -1 to +1 under some conditions (42). They also found that reflection magnitude obtained by the ratio of the amplitudes of the forward and backward pressure waveforms obtained by wave separation (the current gold standard) was more accurate and unaffected by non-linearity (42). However, the traditional approach for calculating reflection magnitude (as the ratio of the amplitudes of the backward and forward pressure waveforms) in theory suffers from the same drawback as the existing return time methods, in that differing reflection patterns could result in the same reflection magnitude and the distributed nature of wave reflection is not accounted for. Thus, future studies could investigate the ratio of the pressure-axis centroids of the backward pressure waveform and input pressure as an index of reflection magnitude.

In conclusion, we have presented a novel centroid method for estimating the bulk return time of backward waves and have shown its greater accuracy, precision and robustness compared to current methods using virtual and animal experiments. This method is therefore likely to provide accurate insights into changes in wave reflection timing that occur in settings such as childhood growth, adult ageing, and disease conditions.

Disclosures

The authors declare no competing interests.

Grants

J.P.M. was supported by a co-funded Career Development Fellowship from the National Health and Medical Research Council of Australia (APP1143510) and Future Leader Fellowship from the National Heart Foundation of Australia (101199). The Heart Research group at the Murdoch Children's Research Institute is supported by the Victorian Government's Operational Infrastructure Program, RCH 1000 and Big W.

References

1. Segers P, Mynard J, Taelman L, Vermeersch S, Swillens A. Wave reflection: Myth or reality? Artery Res. 2012;6(1):7-11.
2. Manisty C, Mayet J, Tapp RJ, Parker KH, Sever P, Poulter NH, et al. Wave Reflection Predicts Cardiovascular Events in Hypertensive Individuals Independent of Blood Pressure and Other Cardiovascular Risk Factors: An ASCOT (Anglo-Scandinavian Cardiac Outcome Trial) Substudy. J Am Coll Cardiol. 2010;56(1):24-30.
3. Nichols WW, O'Rourke MF. McDonald's blood flow in arteries: theoretical, experimental, and clinical principles. O'Rourke MF, Hartley C, McDonald DABfia, editors. London : New York: Oxford University Press; 1998.
4. O'Rourke MF, Hashimoto J. Mechanical factors in arterial aging: a clinical perspective. J Am Coll Cardiol. 2007;50(1):1-13.
5. Chirinos JA, Segers P, Hughes T, Townsend R. Large-Artery Stiffness in Health and Disease: JACC State-of-the-Art Review. J Am Coll Cardiol. 2019;74(9):1237-63.
6. Levy D, Larson MG, Vasan RS, Kannel WB, Ho KKL. The Progression From Hypertension to Congestive Heart Failure. JAMA. 1996;275(20):1557-62.
7. Chirinos JA. Deep Phenotyping of Systemic Arterial Hemodynamics in HFpEF (Part 2): Clinical and Therapeutic Considerations. J Cardiovasc Transl Res. 2017;10(3):261-74.
8. Mitchell GF, Parise H, Benjamin EJ, Larson MG, Keyes MJ, Vita JA, et al. Changes in arterial stiffness and wave reflection with advancing age in healthy men and women: the Framingham Heart Study. Hypertension. 2004;43(6):1239-45.
9. Baksi AJ, Treibel TA, Davies JE, Hadjiloizou N, Foale RA, Parker KH, et al. A meta-analysis of the mechanism of blood pressure change with aging. J Am Coll Cardiol. 2009;54(22):2087-92.
10. Karamanoglu M, Feneley MP. Late systolic pressure augmentation: role of left ventricular outflow patterns. Am J Physiol. 1999;277(2).
11. Hughes AD, Park C, Davies J, Francis D, Mc GTSA, Mayet J, et al. Limitations of augmentation index in the assessment of wave reflection in normotensive healthy individuals. PLoS One. 2013;8(3):e59371.
12. Cheng LT, Tang LJ, Cheng L, Huang HY, Wang T. Limitation of the augmentation index for evaluating arterial stiffness. Hypertens Res. 2007;30(8):713-22.
13. Namasivayam M, Adji A, O'Rourke MF. Aortic Augmentation Index and Aging: Mathematical Resolution of a Physiological Dilemma? Hypertension. 2010;56(1):e9-e10.
14. Heusinkveld MHG, Delhaas T, Lumens J, Huberts W, Spronck B, Hughes AD, et al. Augmentation index is not a proxy for wave reflection magnitude: mechanistic analysis using a computational model. J Appl Physiol (1985). 2019;127(2):491-500.
15. Westerhof N, Sipkema P, van den Bos GC, Elzinga G. Forward and backward waves in the arterial system. Cardiovasc Res. 1972;6(6):648-56.
16. Parker KH. An introduction to wave intensity analysis. Med Biol Eng Comput. 2009;47(2):175.
17. Segers P, Rietzschel ER, De Buyzere ML, De Bacquer D, Van Bortel LM, De Backer G, et al. Assessment of pressure wave reflection: getting the timing right! Physiol Meas. 2007;28(9):1045-56.

18. Torjesen AA, Wang N, Larson MG, Hamburg NM, Vita JA, Levy D, et al. Forward and Backward Wave Morphology and Central Pressure Augmentation in Men and Women in the Framingham Heart Study. Hypertension. 2014;64(2):259-65.
19. Westerhof BE, Westerhof N. Magnitude and return time of the reflected wave: the effects of large artery stiffness and aortic geometry. J Hypertens. 2012;30(5):932-9.
20. Tijsseling AS. Johannes von Kries and the History of Water Hammer. J Hydraul Eng. 2007;133(1):1.
21. Phan TS, Li JKJ, Segers P, Chirinos JA. Misinterpretation of the Determinants of Elevated Forward Wave Amplitude Inflates the Role of the Proximal Aorta. J Am Heart Assoc. 2016;5(2):e003069.
22. Mynard JP, Smolich JJ. Wave potential and the one-dimensional windkessel as a wave-based paradigm of diastolic arterial hemodynamics. Am J Physiol Heart Circ Physiol. 2014;307(3):H307-18.
23. Hametner B, Kastinger H, Wassertheurer S. Simulating re-reflections of arterial pressure waves at the aortic valve using difference equations. Proc Inst Mech Eng H. 2020;234(11):1243-52.
24. Berger DS, Li JK, Laskey WK, Noordergraaf A. Repeated reflection of waves in the systemic arterial system. Am J Physiol Heart Circ Physiol. 1993;264(1):H269-81.
25. Murgo JP, Westerhof N, Giolma JP, Altobelli SA. Aortic input impedance in normal man: relationship to pressure wave forms. Circulation. 1980;62(1):105-16.
26. Chiu YC, Arand PW, Shroff SG, Feldman T, Carroll JD. Determination of pulse wave velocities with computerized algorithms. Am Heart J. 1991;121(5):1460-70.
27. Kondiboyina A, Harrington HA, Smolich JJ, Cheung MMH, Mynard JP. Optimised Design of An Arterial Network Model Reproduces Characteristic Central and Peripheral Hemodynamic Waveform Features in Young Adults. Preprints. 2022;2022030230(doi: 10.20944/preprints202203.0230.v1).
28. Papageorgiou GL, Jones BN, Redding VJ, Hudson N. The area ratio of normal arterial junctions and its implications in pulse wave reflections. Cardiovasc Res. 1990;24(6):478-84.
29. Wang JJ, Parker KH. Wave propagation in a model of the arterial circulation. J Biomech. 2004;37(4):457-70.
30. Alastruey J, Parker K, Peiró J, Sherwin S. Analysing the pattern of pulse waves in arterial networks: a time-domain study. J Eng Math. 2009;64(4):331-51.
31. Mynard JP, Smolich JJ. One-Dimensional Haemodynamic Modeling and Wave Dynamics in the Entire Adult Circulation. Ann Biomed Eng. 2015;43(6):1443-60.
32. Kondiboyina A, Smolich JJ, Cheung MMH, Westerhof BE, Mynard JP. Conduit arterial wave reflection promotes pressure transmission but impedes hydraulic energy transmission to the microvasculature. Am J Physiol Heart Circ Physiol. 2020;319(1):H66-H75.
33. The Reference Values for Arterial Stiffness Collaboration. Determinants of pulse wave velocity in healthy people and in the presence of cardiovascular risk factors: 'establishing normal and reference values'. European Heart Journal. 2010;31(19):2338-50.
34. Rylski B, Desjardins B, Moser W, Bavaria JE, Milewski RK. Gender-related changes in aortic geometry throughout life. Eur J Cardiothorac Surg. 2014;45(5):805-11.
35. Mynard JP, Penny DJ, Smolich JJ. Accurate automatic detection of end-diastole from left ventricular pressure using peak curvature. IEEE Trans Biomed Eng. 2008;55(11):2651-7.
36. O'Rourke MF, Pauca AL. Augmentation of the aortic and central arterial pressure waveform. Blood Press Monit. 2004;9(4):179-85.

37. Sharman JE, Davies JE, Jenkins C, Marwick TH. Augmentation Index, Left Ventricular Contractility, and Wave Reflection. Hypertension. 2009;54(5):1099-105.
38. Wilkinson IB, MacCallum H, Flint L, Cockcroft JR, Newby DE, Webb DJ. The influence of heart rate on augmentation index and central arterial pressure in humans. J Physiol. 2000;525(1):263-70.
39. Segers P, Kips J, Trachet B, Swillens A, Vermeersch S, Mahieu D, et al. Limitations and pitfalls of non-invasive measurement of arterial pressure wave reflections and pulse wave velocity. Artery Res. 2009;3(2):79.
40. Westerhof N. Snapshots of hemodynamics: Springer; 2018.
41. Alastruey J, Hunt AAE, Weinberg PD. Novel wave intensity analysis of arterial pulse wave propagation accounting for peripheral reflections. Int J Num Meth Biomed Eng. 2014;30(2):249-79.
42. Mynard J, Penny DJ, Smolich JJ. Wave intensity amplification and attenuation in non-linear flow: Implications for the calculation of local reflection coefficients. J Biomech. 2008;41(16):3314-21.
43. McEniery CM, Yasmin, Hall IR, Qasem A, Wilkinson IB, Cockcroft JR. Normal vascular aging: differential effects on wave reflection and aortic pulse wave velocity: the Anglo-Cardiff Collaborative Trial (ACCT). J Am Coll Cardiol. 2005;46(9):1753-60.
44. Mynard JP, Harrington HA, Kowalski R, Glenning J, Kondiboyina A, Smolich JJ, et al. Suitability of a representative aortic flow waveform for pressure-only wave separation in children and adolescents. Artery Res. 2021;27:S22.

Tables

Table 1: Characteristics of sheep included in the animal experiment (n = 10). Data is presented as mean ± SD.

Characteristic	Units	Value
Weight	kg	35.3 ± 2.8
Heart Rate	beats/min	107 ± 12
Systolic Blood Pressure	mmHg	78 ± 9
Diastolic Blood Pressure	mmHg	63 ± 11
Cardiac Output	L/min	2.67 ± 0.86

Figures

Figure 1: Estimation of backward wave return time via the (a) inflection point, (b) zero crossing, and (c) foot methods.

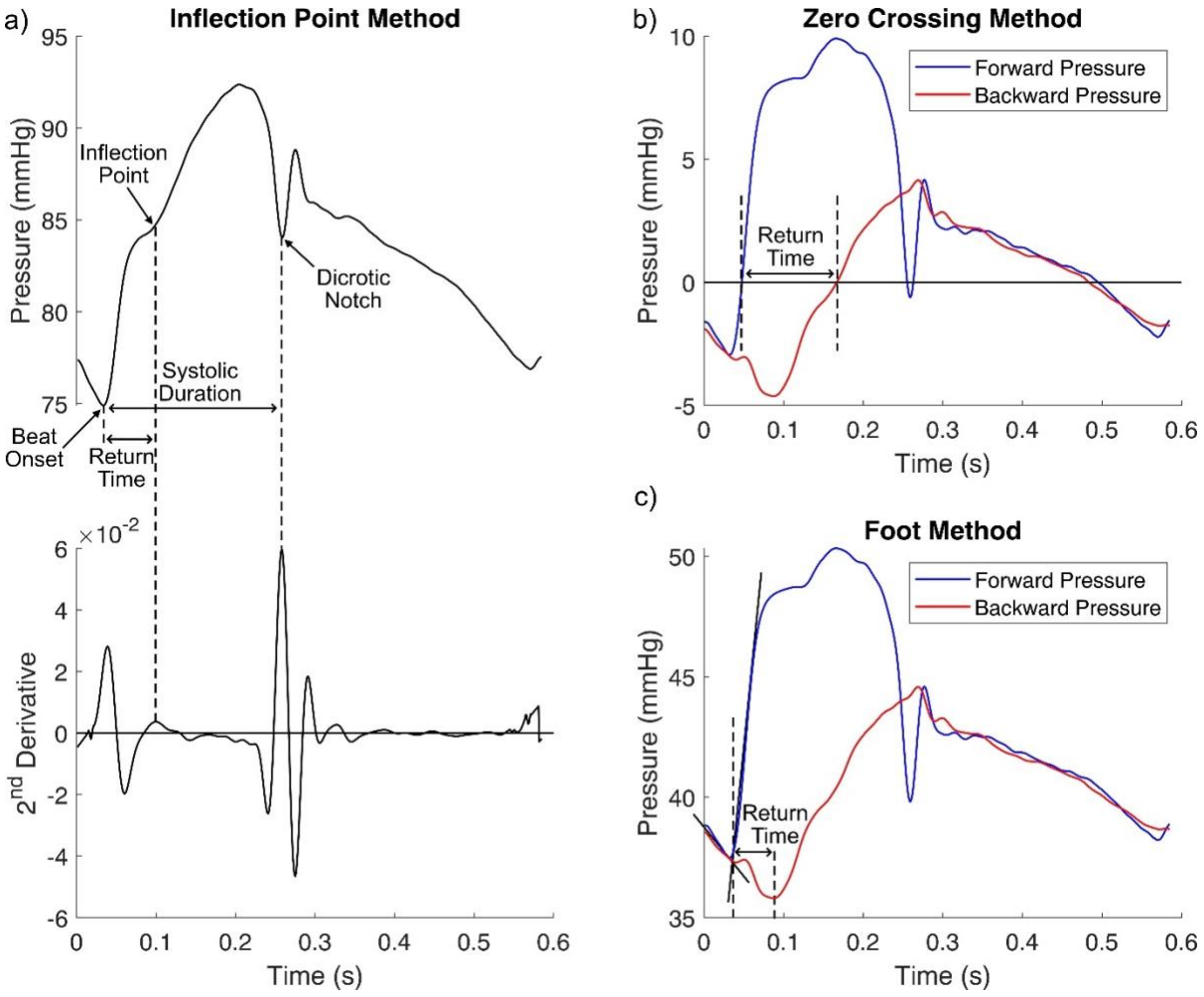

Figure 2: Description of the centroid method. The centroids of the input (blue dashed line) and backward (red dashed line) pressure waveforms are determined by considering the area under the curves from the start of the 1st beat to that of the 2nd beat. The difference between the two centroids is taken as the return time by the centroid method. The time difference between beat onset of the pressure waveform (black dashed line) and the dicrotic notch (black dashed line) is taken as the systolic duration. The black arrow denotes the return time relative to beat onset and thus represents when the "bulk" of the backward pressure waveform arrives. Here, two examples are shown: a) return time is greater than systolic duration and thus the "bulk" backward pressure waveform predominantly returns during diastole; b) return time is less than systolic duration and thus the "bulk" backward pressure waveform predominantly occurs during systole. Note: Pressure waveforms from the carotid artery of an 18-year-old (a) and 57-year old (b) participant were taken the ACCTIII dataset (43) courtesy of Prof Carmel McEniery, Cambridge University, and the flow waveforms were an average representative aortic waveform scaled to beat onset and dicrotic notch of the pressure waveforms (44).

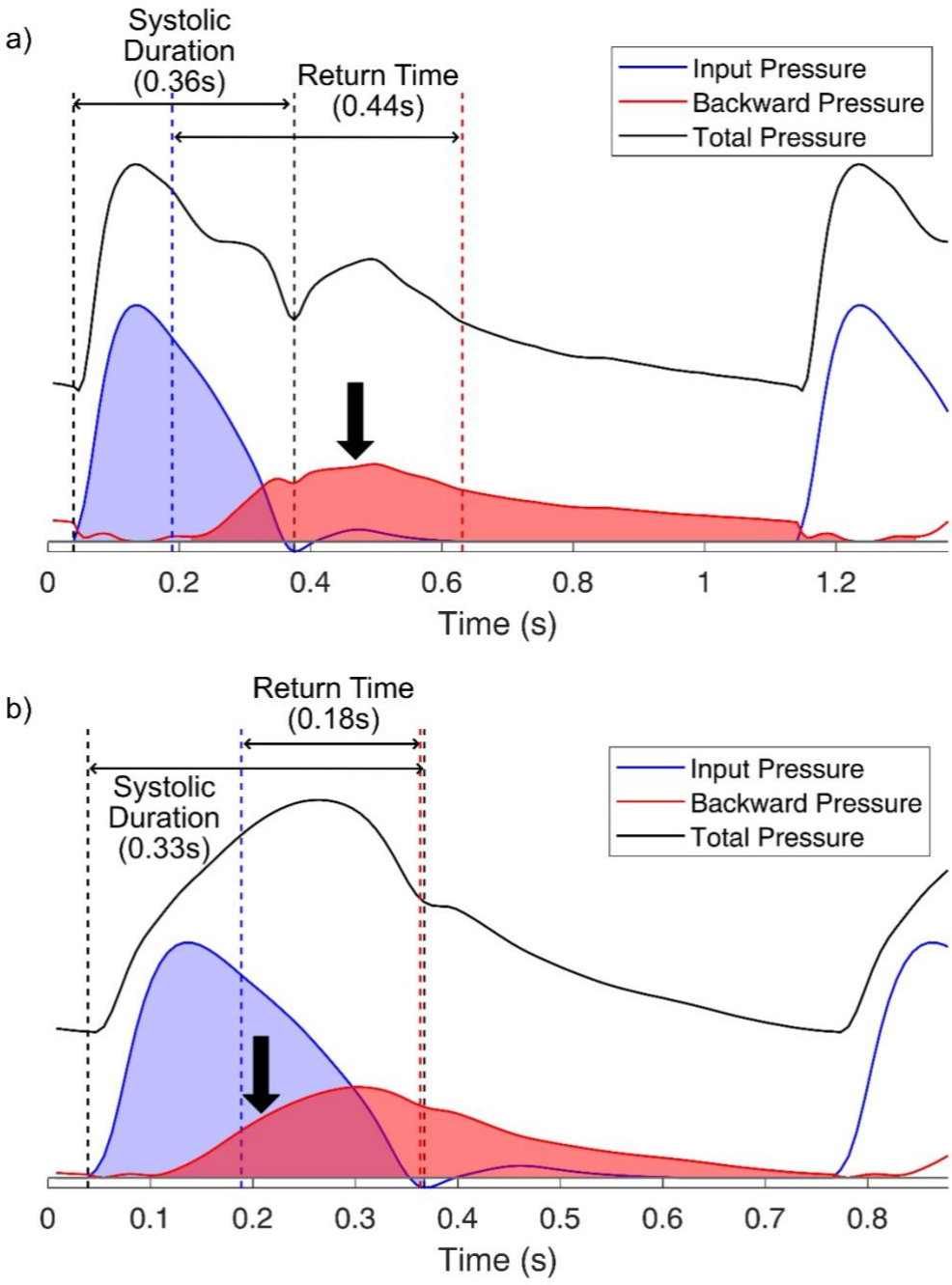
a)
Systolic
Duration
(0.36s)
Return Time
(0.44s)
Input Pressure
Backward Pressure
Total Pressure
0
0.2
0.4
0.6
0.8
1
1.2
Time (s)
b)
Return Time
(0.18s)
Systolic
Duration
(0.33s)
Input Pressure
Backward Pressure
Total Pressure
0
0.1
0.2
0.3
0.4
0.5
0.6
0.7
0.8
Time (s)

Figure 3: Diagrammatic representation of the 1-dimensional model defining parent, daughter, grandparent, and sister vessel terminology. A wave travelling in the parent vessel (a) will be transmitted into the two daughter vessels and reflected back into the parent vessel at its distal end (b). The backward wave in the parent will then be transmitted into the grandparent and sister vessels and reflected back into the parent vessel at its proximal end (c).

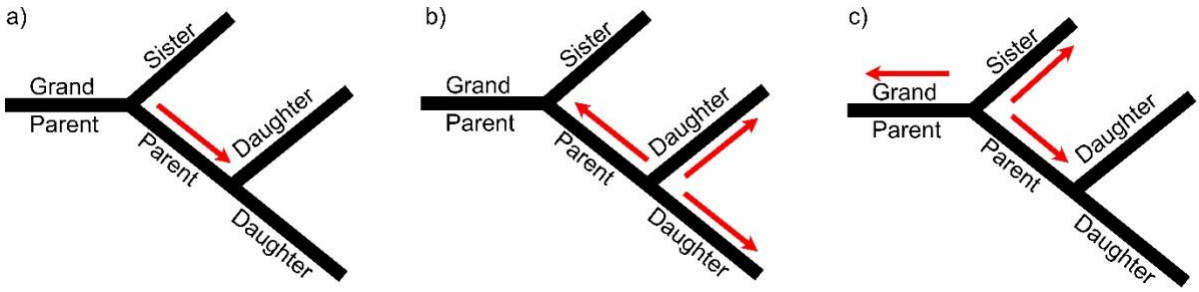

Figure 4: a) The impulse response indicating the timing and amplitude of all waves at the proximal end of the aorta obtained using the linear wave tracking algorithm. The arrow denotes the input impulse of amplitude 1 at time 0. b) The pressure waveform (including the backward and forward pressure waveforms) obtained by convolving the impulse response with an input pressure waveform (shown in blue).

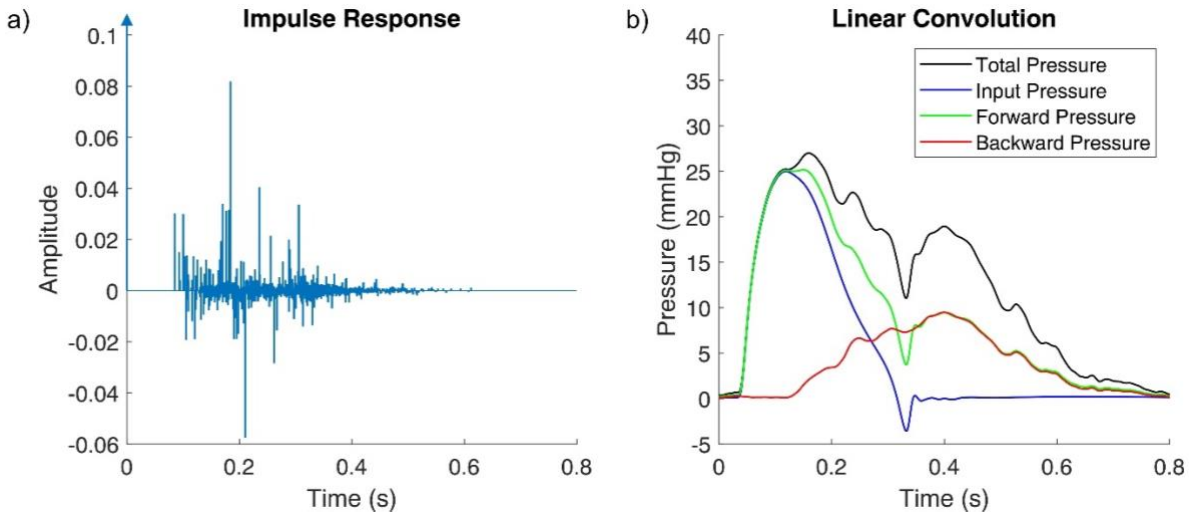

Figure 5: The balloon-induced pulse (BLIP) created by the inflation of the balloon catheter at various times from diastole (bottom) to systole (top) as observed in the pressure waveform in the animal experiments. The red arrows indicate the location of the BLIP on each waveform.

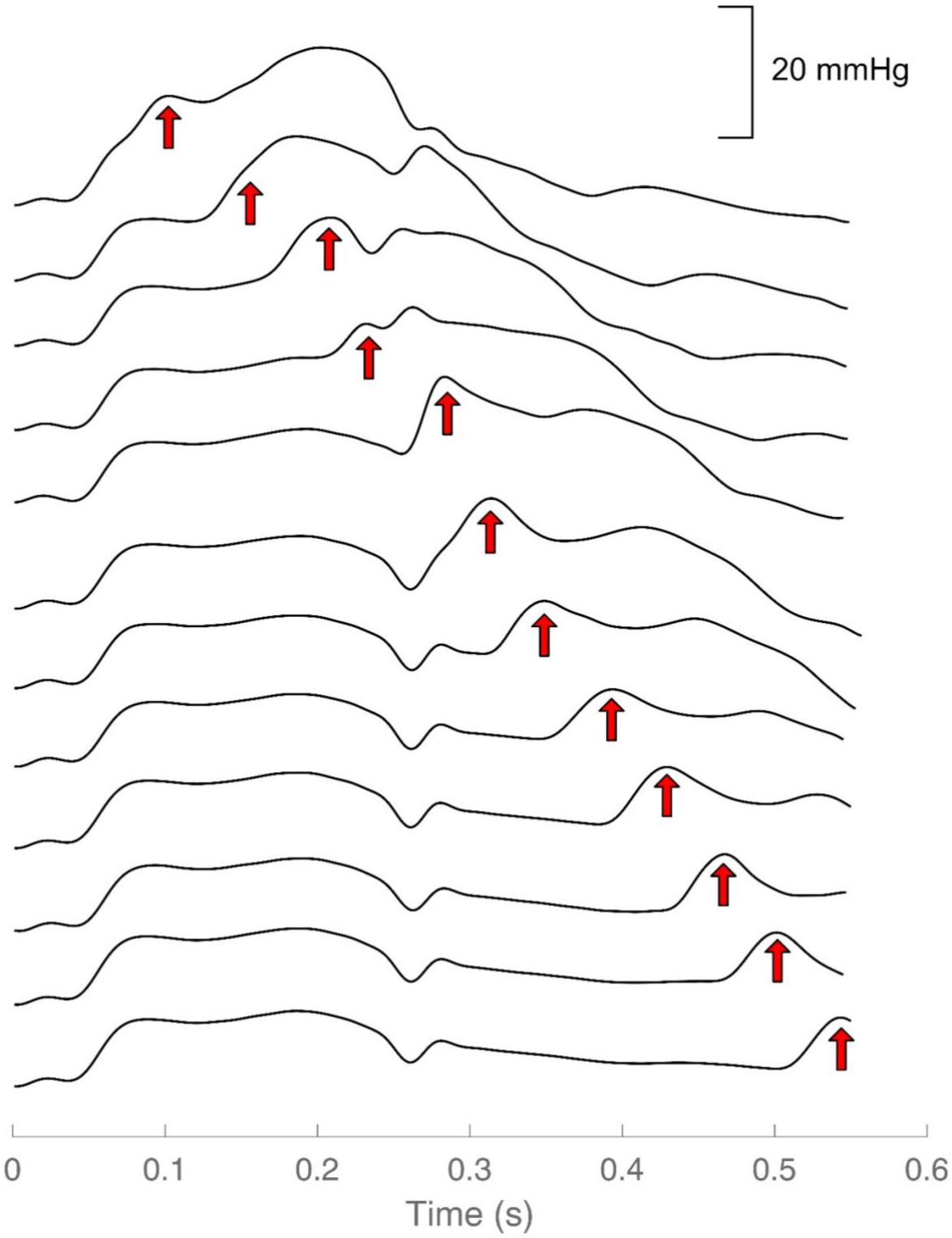

Figure 6: Linear regression analysis of the various methods with the ground truth return time using data from the virtual cohort (black dots). r = correlation coefficient, ICC = intraclass correlation coefficient. The dotted line represents the line of identity (y = x) while the solid red line indicates the linear regression of the data.

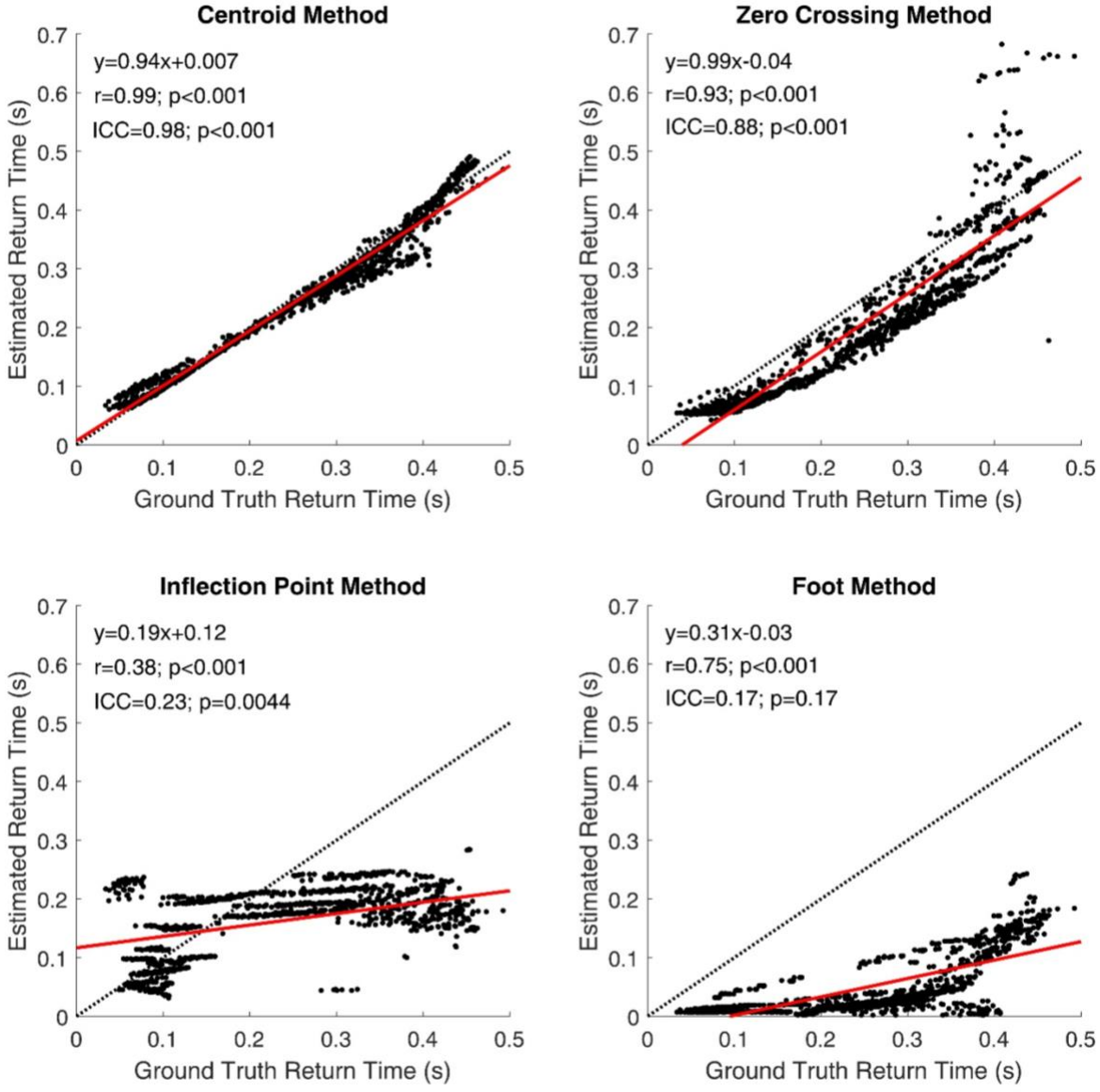

Figure 7: Bland-Altmann analysis of the return time methods indicating the difference between the return time and ground truth return time using data from the virtual cohort. The mean (solid line) $\pm$ 1.96 $\times$ SD (dotted lines) of the differences are shown.

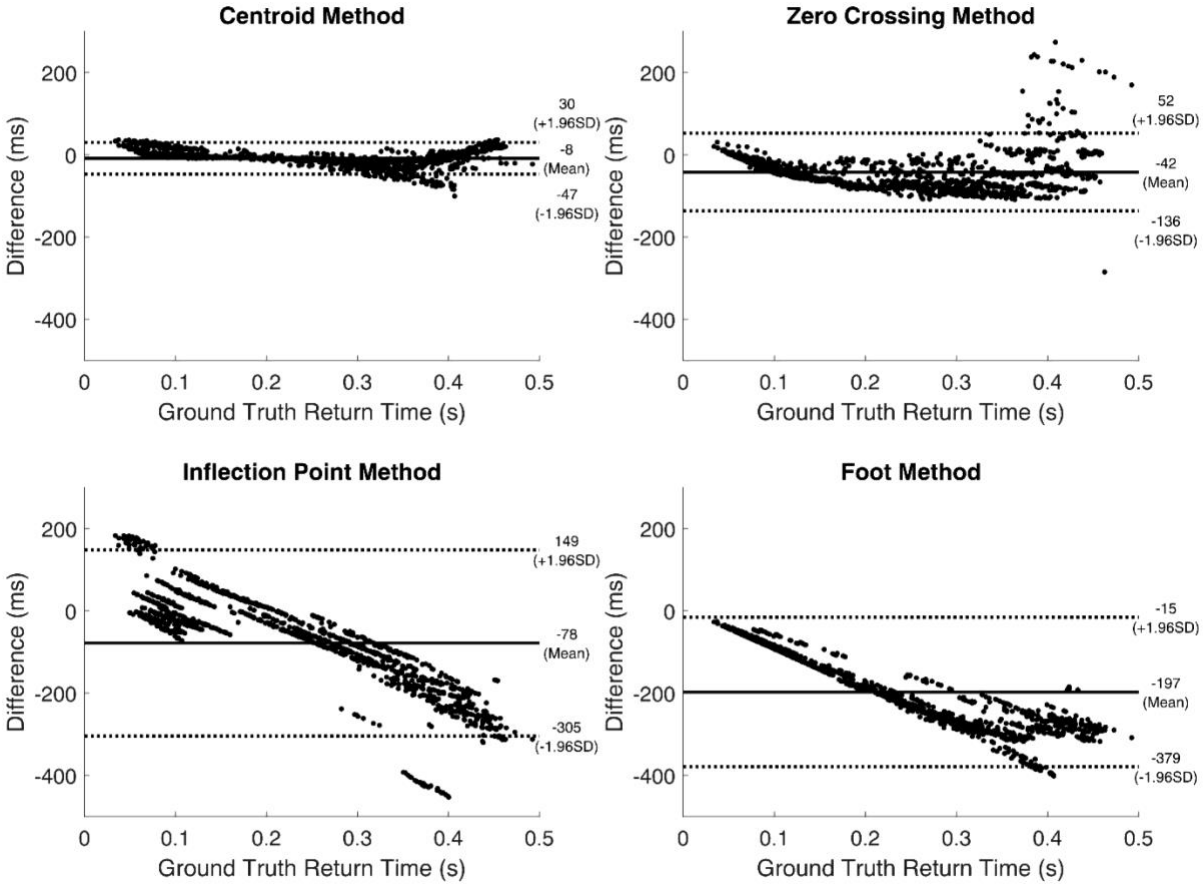

Figure 8: Segmented regression analysis of the return time methods with balloon-induced pulse (BLIP) Index using data from the animal experiments. The breakpoint divides the data into ‘Left’ and ‘Right’ datasets, whose regression equation and corresponding statistics are shown.